Comparison of Orbital and UAV Remote Sensing for Coffee Crop Monitoring in Mountainous Terrain

Igor Araújo Barbosa[1]; Miquéias Henrique Pereira; Daniel Marçal de Queiroz[1]; Andre Luiz de Freitas Coelho[1]; Domingos Sárvio Magalhães Valente[1]; Michel Castro Moreira[1]

[1]Universidade Federal de Viçosa (UFV), Brazil

A paper from the Proceedings of the

17th International Conference on Precision Agriculture and 11th Brazilian Congress on Precision and Digital Agriculture

13-15 July 2026

Porto Alegre, Brazil

Abstract.

Monitoring coffee crops is an important step for the success of production systems. Recently, manual field inspections have been replaced by automated techniques aimed at improving spatial coverage and reducing costs. One such technique is remote sensing, which can be performed using both orbital platforms and Unmanned Aerial Vehicles (UAVs). However, coffee cultivation presents significant imaging challenges due to plant spacing, where wide row spacing results in greater spectral variability compared to annual crops. Furthermore, a wide variety of cultivation techniques are employed. Therefore, it is essential to analyze the performance of different remote sensing platforms in monitoring coffee plantations. This study aimed to compare the spectral characteristics of coffee crops obtained from orbital remote sensing and UAVs using the Sentinel-2 and Planet orbital platforms, and Mavic 3M and Matrice 350 RTK (Micasense RedEdge-P) UAVs. The study compared images in the red, green, and near-infrared bands, which are the most commonly used for calculating vegetation indices. Spatial resolutions were 10 m for Sentinel-2, 3 m for Planet, 5.1 cm for Mavic 3M, and 7.1 cm for Micasense RedEdge-P. The research was conducted across two areas (6.2 ha and 5.4 ha) at Fazenda Oásis in Coimbra, MG, Brazil. UAV images were acquired at a flight altitude of 100 m, and pixels were resampled to ensure comparability with orbital data. Data analysis was based on simple linear regression and on the assessment of the variability of UAV image pixels contained within each satellite image pixel. The R2 values ranged between 0.931 and 0.965 for the spectral bands, demonstrating a strong linear association between orbital and UAV data. Although reflectances were correlated, values differed significantly at many points. Inside each satellite image pixel there is a high variability of reflectance. The red band presented the highest coefficient of variation inside satellite pixels, while the near-infrared band presented the lowest.

Keywords.

Precision Agriculture, Coffee Crop, NDVI, Coffee Crop Reflectance, Vegetation Indices.

1. Introduction

Coffee is among the most important agricultural commodities in the world, sustaining an estimated 125 million jobs predominantly in the tropical regions of South America, Africa, and Asia (Voora et al., 2019). As a perennial crop, coffee production is particularly complex: growers must manage not only yield but also berry quality, since cup quality directly determines market price (Peixoto et al., 2023). This complexity is further compounded by the crop's sensitivity to environmental conditions. Water stress, extreme temperature occurrence, and shifting precipitation patterns associated with climate change can simultaneously reduce productivity and compromise quality (Bilen et al., 2022). Favorable conditions for pests and diseases, such as coffee leaf rust and the coffee berry borer, are closely tied to these same climatic variables, adding yet another layer of management uncertainty (Ferrucho et al., 2024; Aristizábal et al., 2023). Consequently, timely and accurate decision-making across the entire production cycle, from flowering and fruit development through to harvest, is critical. In this context, reliable crop monitoring tools are essential to support farmers in identifying spatial and temporal variability within their fields and implementing site-specific management practices.

Crop monitoring is one of the most challenging activities in precision agriculture, as the soil-plant-atmosphere system is continuously evolving and influencing crop development (Bansod et al., 2017). Traditionally, monitoring relied on visual inspections and field sampling, methods that can be precise but are often labor-intensive, time-consuming, and costly (Bollas et al., 2021). Although aerial photography from manned aircraft was used for agricultural monitoring as early as the 1930s, satellite-based remote sensing was formally adopted in the early 1970s following the launch of Landsat 1 (Phang et al., 2023). Over time, two primary approaches emerged: proximal sensing, in which devices are in direct contact with or in close proximity to the crop, and remote sensing, which relies on sensors mounted on aerial or satellite platforms. Remote sensing generally provides a faster and more cost-effective solution for large-area monitoring compared to proximal approaches (Ebrahimy et al., 2025). The advent of Unmanned Aerial Vehicles (UAVs) has revitalized agricultural remote sensing by enabling centimeter-level spatial resolution and overcoming the cloud cover restrictions that frequently obstruct satellite sensors (Li et al., 2022). Nevertheless, significant challenges remain, including the complexity of radiometric correction and the need for advanced diagnostic models capable of identifying the specific causes of intra-field variability (Hunt Jr. and Daughtry, 2018).

Satellite remote sensing has been applied to a wide range of problems in modern agriculture, drawing on platforms from government missions such as Sentinel-2, Landsat, and MODIS to commercial CubeSat constellations such as PlanetScope (Dubovik et al., 2021). These systems provide multispectral, radar (SAR), and thermal data, enabling high-resolution monitoring of crop development, vigor, and biomass accumulation through indicators such as the Normalized Difference Vegetation Index (NDVI) (Xue et al., 2008). Notable applications include accurate yield prediction for staple grains, drought and flood assessment, and high-precision mapping of nutrient status and foliar diseases such as coffee leaf rust (Martello et al., 2022). The integration of satellite imagery with machine learning and deep learning has further enabled detailed land use and land cover (LULC) classification and the delineation of management zones to optimize irrigation and fertilizer application (Le et al., 2022). Despite these advances, persistent cloud cover and atmospheric interference remain major obstacles, creating temporal data gaps that limit operational utility (Dubovik et al., 2021). Many sensors face an inherent trade-off between spatial resolution and geographic coverage, while smaller commercial satellites may lack stable orbits or on-board calibration systems necessary for consistent long-term records. Remote sensing also remains a fundamentally ill-posed problem: separating the biological signal of interest from background interference, such as soil reflectance or atmospheric absorption. To overcome these barriers complex radiative transfer models and considerable computational resources are necessary (Ghosh et al., 2017). These challenges are particularly acute in heterogeneous or smallholder landscapes, where fragmented fields and high intra-field variability challenge the accuracy of even high-resolution sensors (Kumar et al., 2017).

UAV remote sensing offers distinct advantages over satellite platforms, including centimeter- to millimeter-level spatial resolution, operational flexibility, and the ability to perform customized flight paths and repeated surveys of a target area (Osco et al., 2021). These systems are cost-effective relative to satellite or manned aircraft alternatives and can be readily equipped with a variety of sensors: multispectral, hyperspectral, thermal, and LiDAR. Each type of sensor is tailored to specific research requirements. Flying at low altitudes reduces atmospheric interference and makes UAV systems accessible even to smallholder farmers (Cao et al., 2023). However, notable limitations persist. Battery capacity constrains flight duration and necessitates trade-offs between propulsion and onboard data processing. Varying illumination conditions caused by fluctuating cloud cover or changing solar angles introduce spectral inconsistencies that require rigorous radiometric calibration to resolve (Wang et al., 2024). Furthermore, the large volumes of high-resolution data generated by UAV platforms can create significant processing bottlenecks, particularly on resource-constrained hardware (Huang et al., 2025).

Selecting the most appropriate remote sensing system for a given application is not an easy task. Coffee cultivation in mountainous terrain presents a particular set of challenges, including complex topography, fragmented fields, and variable illumination, that make this choice especially consequential. The objective of this study is therefore to compare orbital and UAV remote sensing systems for monitoring coffee crops grown in mountainous areas, assessing their respective performance, limitations, and practical suitability for precision agriculture applications in this environment.

2. Material and Methods

This work was conducted at Fazenda Oásis, located in the municipality of Coimbra, state of Minas Gerais, Brazil. Two areas were selected for the study, both characterized by mountainous terrain. Area 1, covering 6.2 ha (Figures 1a and 1b), has mean slope of 28.5%, while Area 2, covering 5.4 ha (Figure 1c and 1d), presents mean slope of 25.6%.

The areas were imaged using two platforms: (a) a DJI Matrice 350 RTK unmanned aerial vehicle (UAV) equipped with a Micasense RedEdge-P camera, and (b) a DJI Mavic 3M UAV equipped with its multispectral camera. Images were acquired on September 11, 2025. Flights were conducted at an altitude of 100 m above ground level following terrain relief, resulting in a ground sampling distance of 5.1 cm for the Mavic 3M multispectral camera and 7.1 cm for the Micasense RedEdge-P camera. Given the mountainous terrain, front and side overlap were both set to 85%. Radiometric calibration was performed using a Calibrated Reflectance Panel (model RP06, Micasense, Seattle, WA, USA), which has a calibration surface of 100 mm × 100 mm. Prior and after to each flight, the UAV camera was positioned approximately 1 m above the panel to capture calibration images. Images from both cameras were processed using Pix4D Mapper software, version 4.9.0 (Pix4D, Lausanne, Switzerland).

Planet imagery, with a pixel size of 3 m, was acquired for both areas on September 11, 2025. Sentinel-2 imagery, with a pixel size of 10 m, was acquired on September 4, 2025.

For both UAV and satellite imagery, the red, green, and near-infrared bands were analyzed. To enable comparison between UAV and satellite images, UAV imagery was resampled to match the pixel size of each satellite sensor. A custom script was developed in Python (version 3.10) for this purpose, using the rasterio module to perform the resampling. Table 1 presents the wavelengths of the three bands for all the imaging sensors used in this work.

In addition to comparing reflectance values in the green, red, and near-infrared bands between UAV and satellite imagery, the Normalized Difference Vegetation Index (NDVI) was also compared. For the satellite imagery, the variability in reflectance and NDVI captured by each of the two UAV platforms was also assessed.

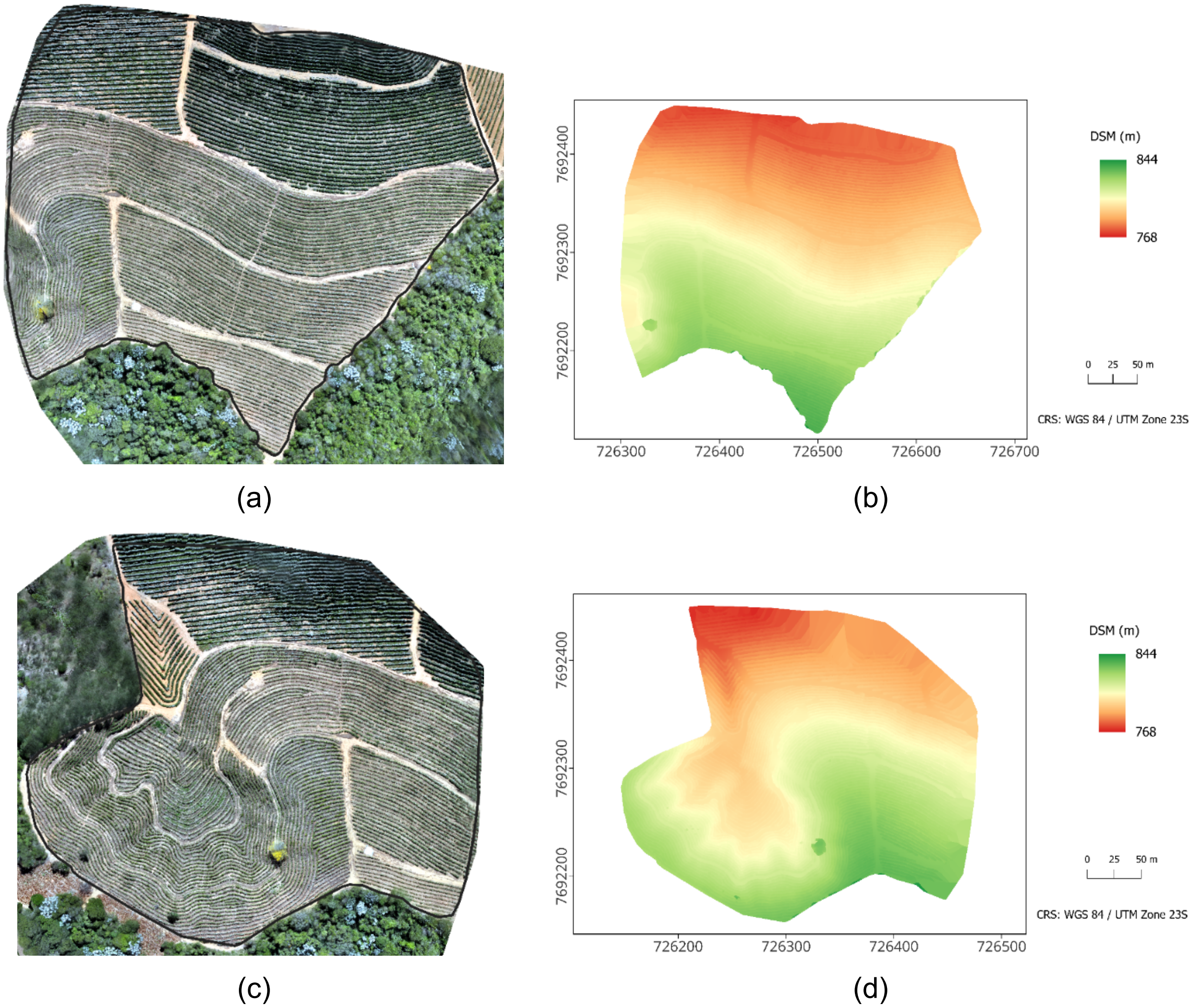

Figure 1 – Characteristics of the coffee fields where the images were collected. (a) mosaic of the Area 1; (b) Digital elevation map of Area 1; (c) mosaic of the Area 2; (d) Digital elevation map of Area 2.

Table 1 – Characteristics of Planet, Sentinel 2, Mavic 3M and Micasense Red-Edge-P for the red, green and near infrared (NIR) bands

Bands	Characteristics	Planet	Sentinel 2	Mavic 3M	Micasense RedEdge-P
Green	Central wavelength (nm)	565	559.8	560	560
	Band width (nm)	36	35	16	27
Red	Central wavelength (nm)	665	664.6	650	668
	Band width (nm)	31	30	16	16
NIR	Central wavelength (nm)	865	864.7	860	842
	Band width (nm)	40	21	26	57

Sources: Planet (2019), CDSE (2026), Micasense (2026), DJI Agriculture (2026)

3. Results and Discussion

Figure 2 presents the comparison of the reflectance obtained by the Planet images of the coffee fields and the reflectance obtained by using Mavic 3M multispectral camera and by Micasense RedEdge-P multispectral camera. Because the ground sampling distance of the UAV images differed from that of the Planet images, the UAV images were resampled to match the satellite pixel size. There was a good agreement between Planet and UAV images. There was no evident difference between both multispectral cameras when compared to Planet images. Also, there was no difference between the results of coffee field Area 1 (mountainous with gentler relief) and Area 2 (mountainous with steeper terrain).

Coffee is cultivated with a row spacing of three to four meters. Therefore, the pixel of a satellite image is not uniform, it is a mixture of coffee row and interrow areas. Tables 2 and 3 show the variability of the green, red, and NIR bands within a Planet pixel, as determined using UAV images. The red band presented the highest mean coefficient of variation inside the pixels, because a large difference between coffee row and interrow reflectance is expected in the red band. Coffee row reflectance is much lower than the soil reflectance because of the chlorophyll red band absorption. The NIR band presented the lowest coefficient of variation among the bands, because the difference in NIR reflectance between coffee rows and interrows is smaller than for the red band.

Figure 3 presents a comparison of the reflectance obtained by the Sentinel 2 images of the coffee fields and the reflectance obtained by using Mavic 3M multispectral camera and by Micasense RedEdge-P multispectral camera. The pixel size of Sentinel 2 images is 10 m and Planet is 3 m. As the pixel size of Sentinel 2 covers a larger area than the Planet pixel, the number of data points was lower than in Figure 2. There was good agreement between the reflectance obtained using Sentinel 2 and both UAV multispectral cameras.

Tables 4 and 5 show the analysis of variability inside each Sentinel 2 pixel. The results were similar to those obtained for the Planet pixels. The red band had the highest mean coefficient of variation, and the NIR band presented the lowest. There was no difference between the two coffee fields.

Figures 4 and 5 present the comparison of the NDVI obtained from UAV multispectral images with Planet and Sentinel images, respectively. The agreement between the imaging platforms was lower than for the results obtained with the green, red, and NIR bands (Figures 2 and 3). This is because NDVI is computed from a combination of the red and NIR bands. Also, the analysis was performed using the entire dataset, and the plots indicate the need for an outlier analysis. Some NDVI values obtained from the UAV images appear unrealistic; for instance, a coffee field should not present NDVI values lower than 0.15, which indicates exposed soil, yet the plots show data points in this range.

The results obtained in this work showed a good agreement between satellite imagery (Planet and Sentinel 2) and UAV multispectral camera (Mavic 3M and Micasense RedEdge-P multispectral cameras). This means that good results can be obtained using satellite imagery. However, the results also demonstrated that inside a pixel of a satellite image there is a high variability of reflectance values, the lowest coefficient of variation was 22% for the NIR band and the highest coefficient of variation was higher than 50% for the red band. Therefore, the pixel of a coffee crop area of a satellite image does not show the real spatial variability occurring in the field.

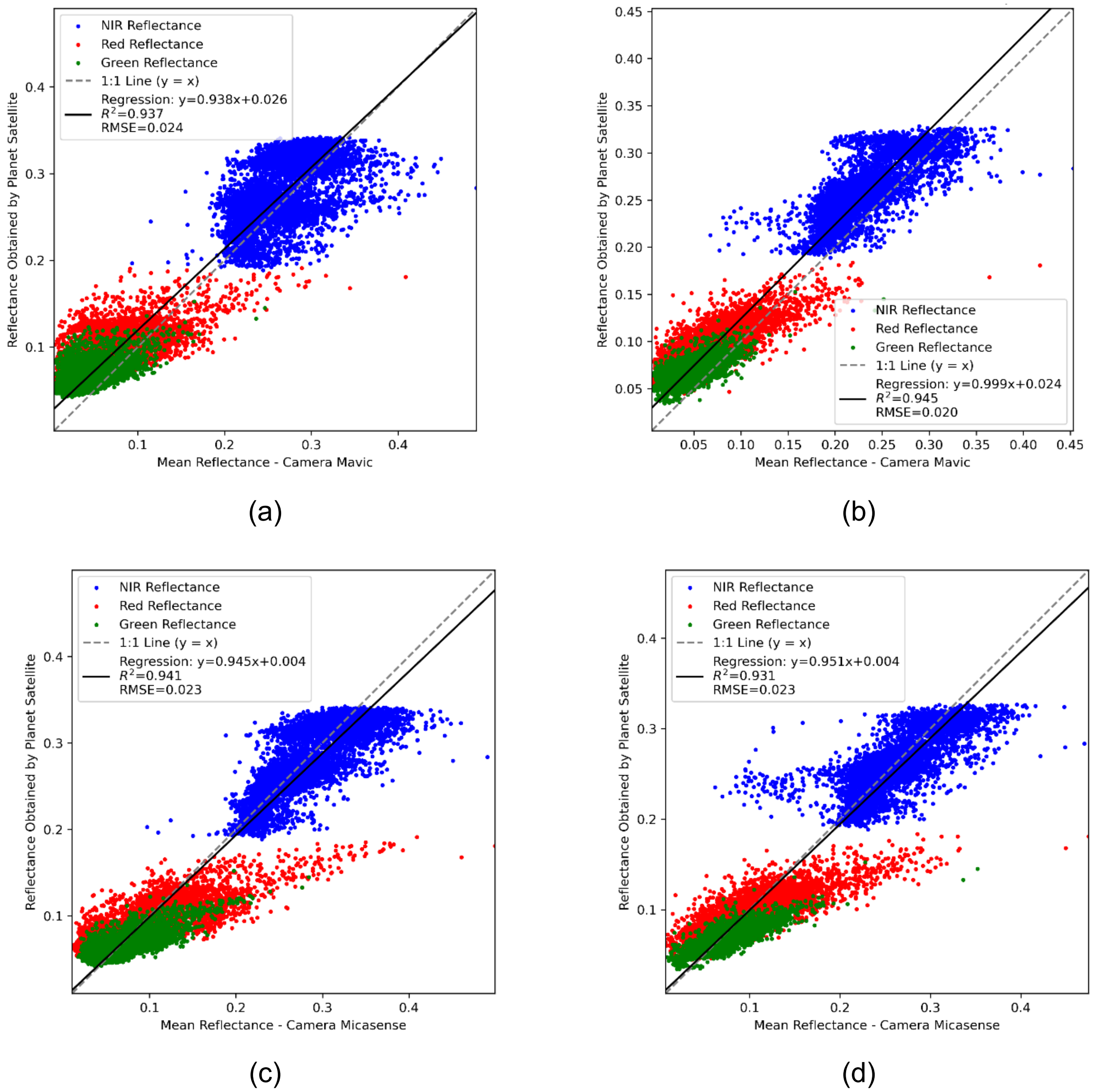

Figure 2 – Comparison between reflectance values in the green, red and NIR bands obtained by the Planet satellite and by the Micasense RedEdge-P and Mavic Multispectral cameras. (a) Planet vs Mavic Multispectral in Area 1, (b) Planet vs Mavic Multispectral in Area 2, (c) Planet vs Micasense RedEdge-P in Area 1, (d) Planet vs Micasense RedEdge-P in Area 2.

Table 2 – Reflectance variability analysis inside the Planet images pixel using Mavic 3M camera

		Planet image		Mavic 3M camera		
Reflectance band	Coffee field	Number of pixels	Mean reflectance	Mean reflectance	Mean standard deviation inside Planet pixel	Mean coefficient of variation (%) inside Planet pixel
Green	Area 1	9086	0.065	0.049	0.024	25.69
	Area 2	7103	0.068	0.050	0.015	32.57
Red	Area 1	9086	0.089	0.068	0.026	45.12
	Area 2	7103	0.096	0.072	0.026	38.69
NIR	Area 1	9086	0.273	0.259	0.069	26.25
	Area 2	7103	0.259	0.228	0.051	22.30

Table 3 - Reflectance variability analysis inside the Planet images pixel using Micasense RedEdge-P camera

		Planet image		Micasense RedEdge-P camera		
Reflectance band	Coffee field	Number of pixels	Mean reflectance	Mean reflectance	Mean standard deviation inside Planet pixel	Mean coefficient of variation (%) inside Planet pixel
Green	Area 1	9049	0.065	0.070	0.023	35.99
	Area 2	7557	0.067	0.073	0.022	31.38
Red	Area 1	9049	0.089	0.093	0.036	46.29
	Area 2	7257	0.096	0.101	0.037	39.84
NIR	Area 1	9049	0.275	0.276	0.076	26.77
	Area 2	7257	0.260	0.259	0.059	22.79

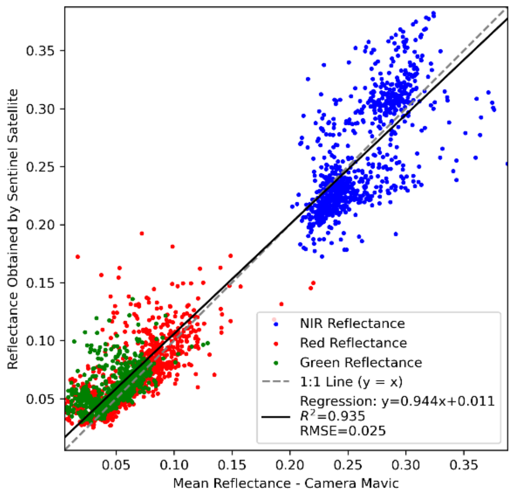

(a)

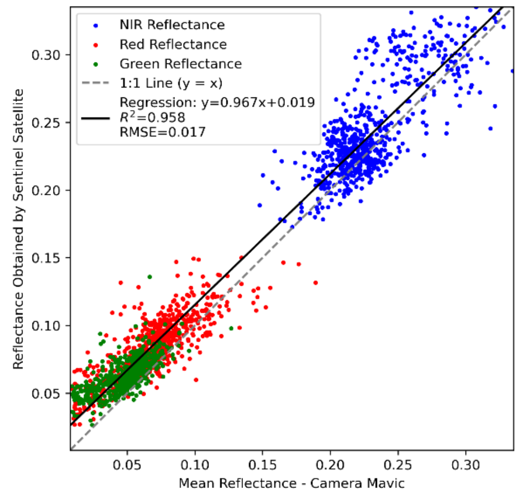

(b)

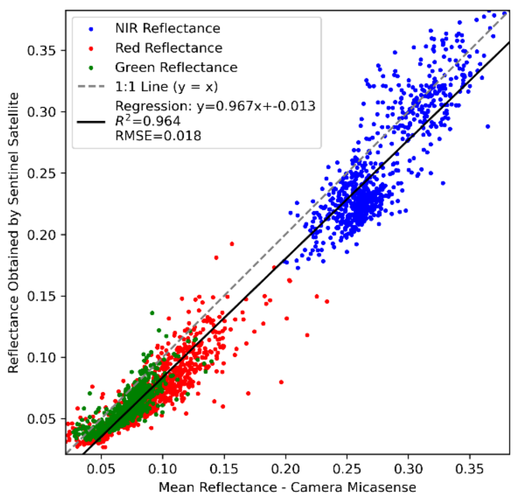

(c)

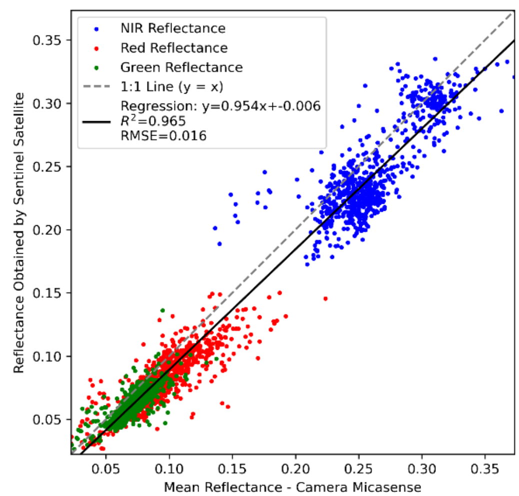

(d)

Figure 3 – Comparison between reflectance values in the green, red and NIR bands obtained by the Sentinel 2 satellite and by the Micasense RedEdge-P and Mavic Multispectral cameras. (a) Sentinel 2 vs Mavic Multispectral in Area 1, (b) Sentinel 2 vs Mavic Multispectral in Area 2, (c) Sentinel 2 vs Micasense RedEdge-P in Area 1, (d) Sentinel 2 vs Micasense RedEdge-P in Area 2.

Table 4 - Reflectance variability analysis inside the Sentinel 2 images pixel using Mavic 3M camera

Reflectance band	Coffee field	Sentinel 2 image: Number of pixels	Sentinel 2 image: Mean reflectance	Mavic 3M camera: Mean reflectance	Mavic 3M camera: Mean standard deviation inside Sentinel 2 pixel	Mavic 3M camera: Mean coefficient of variation (%) inside Sentinel 2 pixel
Green	Area 1	839	0.058	0.049	0.018	41.30
	Area 2	664	0.064	0.049	0.017	37.26
Red	Area 1	839	0.073	0.067	0.031	51.70
	Area 2	664	0.086	0.070	0.029	45.52
NIR	Area 1	839	0.259	0.260	0.074	27.99
	Area 2	664	0.250	0.230	0.057	24.50

Table 5 - Reflectance variability analysis inside the Sentinel 2 images pixel using Micasense RedEdge-P camera

Reflectance band	Coffee field	Sentinel 2 image: Number of pixels	Sentinel 2 image: Mean reflectance	Micasense RedEdge-P camera: Mean reflectance	Micasense RedEdge-P camera: Mean standard deviation inside Sentinel 2 pixel	Micasense RedEdge-P camera: Mean coefficient of variation (%) inside Sentinel 2 pixel
Green	Area 1	848	0.058	0.070	0.027	40.82
	Area 2	708	0.063	0.072	0.026	37.68
Red	Area 1	848	0.073	0.092	0.046	53.92
	Area 2	708	0.084	0.098	0.046	49.02
NIR	Area 1	848	0.259	0.276	0.082	28.42
	Area 2	708	0.246	0.262	0.068	25.81

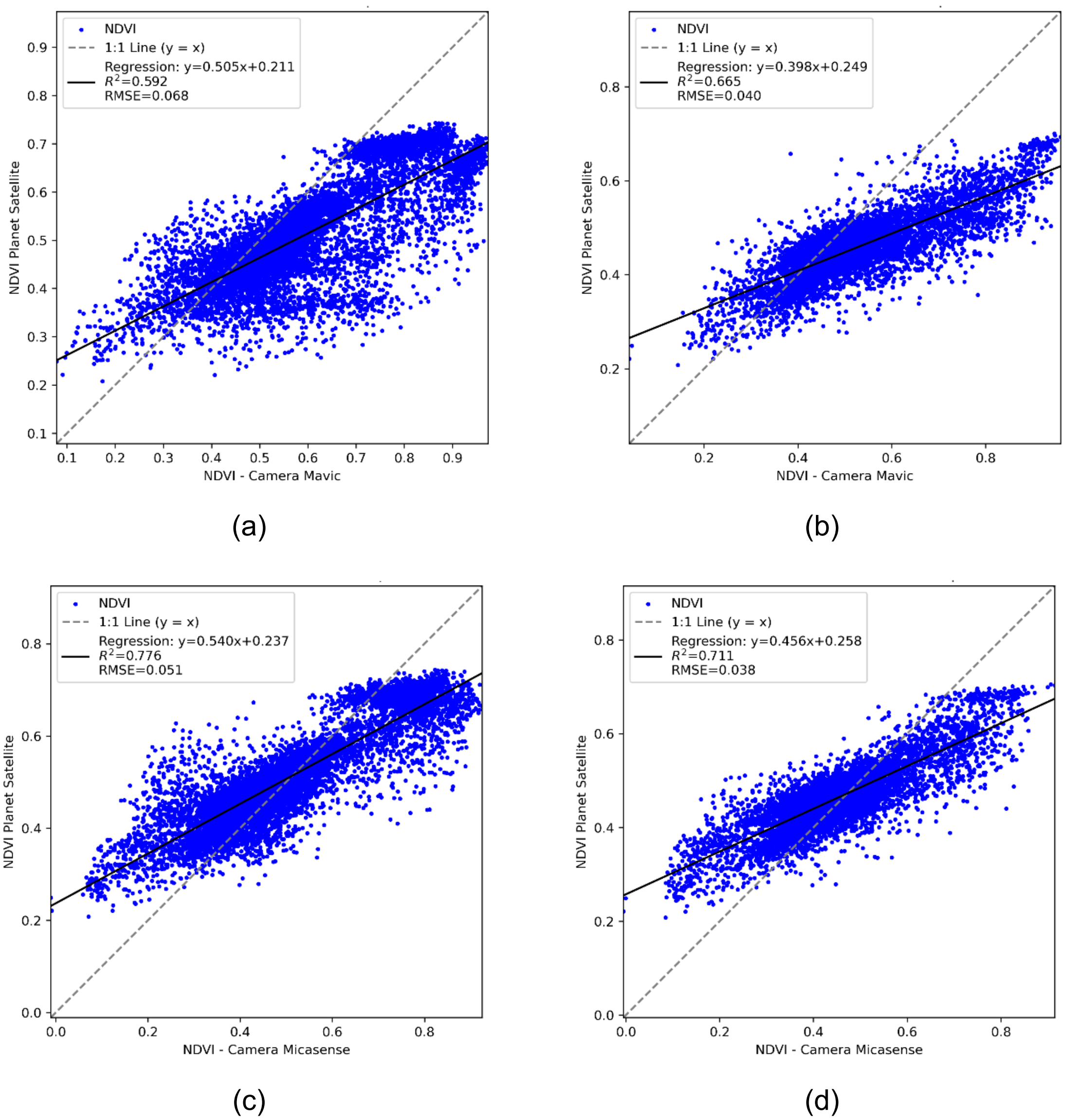

Figure 4 – Comparison between NDVI values calculated from images obtained by the Planet satellite and by the Micasense RedEdge-P and Mavic Multispectral cameras. (a) NDVI Planet vs NDVI Mavic Multispectral in Area 1, (b) NDVI Planet vs NDVI Mavic Multispectral in Area 2, (c) NDVI Planet vs NDVI Micasense RedEdge-P in Area 1, (d) NDVI Planet vs NDVI Micasense RedEdge-P in Area 2.

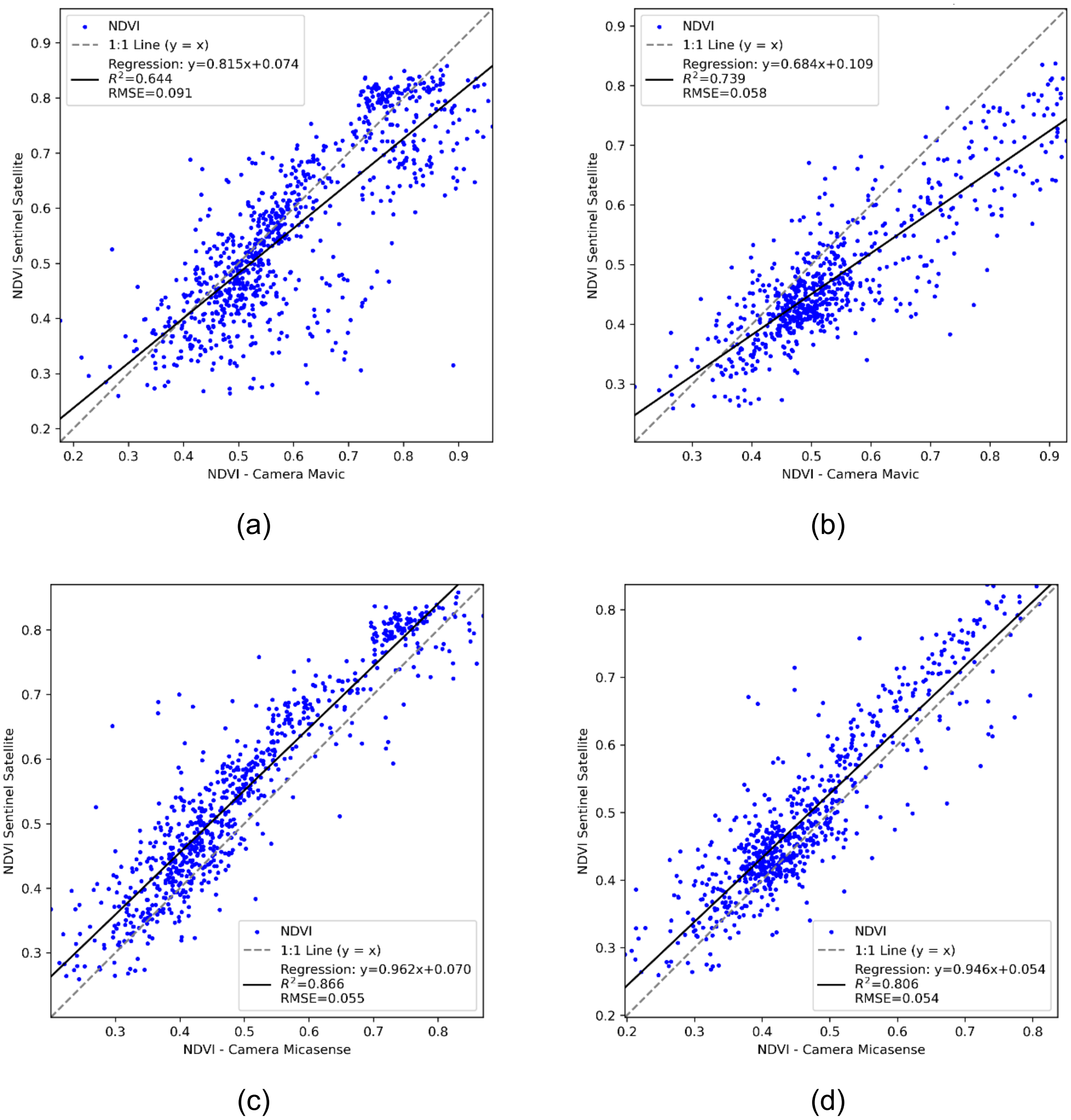

Figure 5 – Comparison between NDVI values calculated from images obtained by the Sentinel 2 satellite and by the Micasense RedEdge-P and Mavic Multispectral cameras. (a) NDVI Sentinel 2 vs NDVI Mavic Multispectral in Area 1, (b) NDVI Sentinel 2 vs NDVI Mavic Multispectral in Area 2, (c) NDVI Sentinel 2 vs NDVI Micasense RedEdge-P in Area 1, (d) NDVI Sentinel 2 vs NDVI Micasense RedEdge-P in Area 2.

4. Conclusions

The reflectance obtained by Planet and Sentinel 2 satellites of coffee fields presented good agreement with the reflectance obtained by using Micasense RedEdge-P and Mavic 3M multispectral cameras for the green, red and NIR bands.

Inside each satellite image pixel there is a high variability of reflectance. The red band presented the highest coefficient of variation inside satellite pixels, while the NIR band presented the lowest.

The NDVI calculated using images of coffee fields obtained by Planet and Sentinel 2 satellites presented good agreement with NDVI obtained by using Micasense RedEdge-P and Mavic 3M multispectral cameras.

5. Acknowledgments

The present study was carried out with support from the Coordination for the Improvement of Higher Education Personnel - Brazil (CAPES) - Funding Code 001, the Minas Gerais State Research Support Foundation - Process APQ-00750-23 (Artificial Intelligence Models from Digital Agriculture Data for Mountain Coffee Crop Management), and the National Council for Scientific and Technological Development - Brazil (CNPq).

6. References

Aristizábal, L. F.; Johnson, M. A.; Mariño, Y. A.; Bayman, P.; & Wright, M. G. (2023). Establishing an integrated pest management program for coffee berry borer (Hypothenemus hampei) in Hawaii and Puerto Rico coffee agroecosystems: achievements and challenges. *Insects*, *14*(7), 603.

Bansod, B.; Singh, R.; Thakur, R.; & Singhal, G. (2017). A comparison between satellite based and drone based remote sensing technology to achieve sustainable development: A review. *Journal of Agriculture and Environment for International Development (JAEID)*, *111*(2), 383-407.

Bollas, N.; Kokinou, E.; & Polychronos, V. (2021). Comparison of sentinel-2 and UAV multispectral data for use in precision agriculture: An application from northern Greece. *Drones*, *5*(2), 35.

Bilen, C.; El Chami, D.; Mereu, V.; Trabucco, A.; Marras, S.; & Spano, D. (2022). A systematic review on the impacts of climate change on coffee agrosystems. *Plants*, *12*(1), 102.

Cao, Z.; Kooistra, L.; Wang, W.; Guo, L.; & Valente, J. (2023). Real-time object detection based on uav remote sensing: A systematic literature review. *Drones*, *7*(10), 620.

CDSE (Copernicus Data Space Ecosystem) (2026). Sentinel-2 Documentation. https://documentation.dataspace.copernicus.eu/Data/SentinelMissions/Sentinel2.html. Accessed on June 10th, 2026.

DJI Agriculture (2026). DJI 3 M specifications. https://ag.dji.com/pt-br/mavic-3-m/specs. Accessed on June 10, 2026.

Dubovik, O.; Schuster, G. L.; Xu, F.; Hu, Y.; Bösch, H.; Landgraf, J.; & Li, Z. (2021). Grand challenges in satellite remote sensing. Frontiers in Remote Sensing, 2, 619818.

Ebrahimy, H.; Yu, T.; & Zhang, Z. (2025). Developing a spatiotemporal fusion framework for generating daily UAV images in agricultural areas using publicly available satellite data. *ISPRS*

Journal of Photogrammetry and Remote Sensing, *220*, 413-427.

Ferrucho, R. L.; Marín-Ramírez, G. A.; & Gaitan, A. (2024). Integrated disease management for the sustainable production of Colombian coffee. *Agronomy*, *14*(6), 1286.

Ghosh, S. M.; Saraf, S.; Behera, M. D.; & Biradar, C. (2017). Estimating agricultural crop types and fallow lands using multi temporal Sentinel-2A imageries. *Proceedings of the National Academy of Sciences, India Section A: Physical Sciences*, *87*(4), 769-779.

Huang, D.; Zhou, Z.; Zhang, Z.; Du, X.; Fan, R.; Li, Q.; & Huang, Y. (2025). From Application-Driven Growth to Paradigm Shift: Scientific Evolution and Core Bottleneck Analysis in the Field of UAV Remote Sensing. *Applied Sciences*, *15*(15), 8304.

Hunt Jr, E. R.; & Daughtry, C. S. (2018). What good are unmanned aircraft systems for agricultural remote sensing and precision agriculture? *International journal of remote sensing*, *39*(15-16), 5345-5376.

Kumar, S.; Garg, R. D.; Kushwaha, S. P. S.; & Pandey, U. (2017). Spaceborne SAR tomography for vertical profile retrieval of forest vegetation. *Proceedings of the National Academy of Sciences, India Section A: Physical Sciences*, *87*(4), 807-816.

Le, Q. T.; Dang, K. B.; Giang, T. L.; Tong, T. H. A.; Nguyen, V. G.; Nguyen, T. D. L.; & Yasir, M. (2022). Deep learning model development for detecting coffee tree changes based on Sentinel-2 imagery in Vietnam. *Ieee Access*, *10*, 109097-109107.

Li, M.; Shamshiri, R. R.; Weltzien, C.; & Schirrmann, M. (2022). Crop monitoring using Sentinel-2 and UAV multispectral imagery: A comparison case study in Northeastern Germany. *Remote Sensing*, *14*(17), 4426.

Martello, M.; Molin, J. P.; Wei, M. C. F.; Canal Filho, R.; & Nicoletti, J. V. M. (2022). Coffee-yield estimation using high-resolution time-series satellite images and machine learning. *AgriEngineering*, *4*(4), 888-902.

Micasense (2026). RedEdge-P Integration Guide. https://support.micasense.com/hc/en-us/articles/4410824602903-RedEdge-P-Integration-Guide. Accessed on June 10, 2026.

Osco, L.P.; Junior, J.M.; Ramos, A.P.M.; Jorge, L.A.C.; Fatholahi, S.N.; Silva, J.A.; Matsubara, E.T.; Pistori, H.; Gonçalves, W.N.; and Li, J. (2021). A review on deep learning in UAV remote sensing. *International Journal of Applied Earth Observation and Geoinformation*, *102*, p.102456.

Peixoto, J. A.B.; Silva, J. F.; Oliveira, M. B. P.; & Alves, R. C. (2023). Sustainability issues along the coffee chain: From the field to the cup. *Comprehensive Reviews in Food Science and Food Safety*, *22*(1), 287-332.

Phang, S. K.; Chiang, T. H. A.; Happonen, A.; & Chang, M. M. L. (2023). From satellite to UAV-based remote sensing: A review on precision agriculture. *Ieee Access*, *11*, 127057-127076.

Planet. (2019) Planet imagery product specifications. *Planet Labs: San Francisco, CA, USA*, *91*, 170.

Voora, V., Bermudez, S., Larrea, C., & Baliño, S. (2019). Global market report: Coffee. International Institute for Sustainable Development, Winnipeg, Canada.

Xue, Y.; Li, Y.; Guang, J.; Zhang, X.; & Guo, J. (2008). Small satellite remote sensing and applications–history, current and future. *International journal of remote sensing*, *29*(15), 4339-4372.